Mixed poly (ethylene glycol) and oligo (ethylene glycol) layers on gold as nonfouling surfaces created by backfilling

Arcot R. Lokanathan, Shuai Zhang, Viduthalai R. Regina, Martin A. Cole, Ryosuke Ogaki,[a)]
Mingdong Dong, Flemming Besenbacher, and Rikke L. Meyer
The Interdisciplinary Nanoscience Centre (iNANO), Aarhus University, Ny Munkegade 120, Aarhus 8000, Denmark

Peter Kingshott[a),b)]
Industrial Research Institute Swinburne (IRIS), Faculty of Engineering and Industrial Sciences, Advanced Technologies Centre (ATC), Swinburne University of Technology, Burwood Road, Hawthorn, Victoria 3122, Australia

Backfilling a self-assembled monolayer (SAM) of long poly (ethylene glycol) (PEG) with short PEG is a well-known strategy to improve its potential to resist fouling. Here it is shown, using x-ray photoelectron spectroscopy, contact angle, and atomic force microscopy, that backfilling PEG thiol with oligo (ethylene glycol) (OEG) terminated alkane thiol molecules results in underbrush formation. The authors also confirm the absence of phase separated arrangement, which is commonly observed with backfilling experiments involving SAMs of short chain alkane thiol with long chain alkane thiol. Furthermore, it was found that OEG addition caused less PEG desorption when compared to alkane thiol. The ability of surface to resist fouling was tested through serum adsorption and bacterial adhesion studies. The authors demonstrate that the mixed monolayer with PEG and OEG is better than PEG at resisting protein adsorption and bacterial adhesion, and conclude that backfilling PEG with OEG resulting in the underbrush formation enhances the ability of PEG to resist fouling. © *2011 American Vacuum Society*. [DOI: 10.1116/1.3647506]

I. INTRODUCTION

Nonfouling coatings are immensely important to a variety of biomedical applications such as implants, drug delivery, tissue engineering, and biosensing.[1] They are also important for water purification, food processing, and marine industries.[2] One goal of a nonfouling coating is to reduce biofilm formation on surfaces while maintaining functionality. Biofilm formation is found to be facilitated by a conditioning layer (adsorbed layer of biomolecules from the surrounding environment), which is followed by reversible physiochemical attachment of microbes.[3] Among the various strategies used in making nonfouling coatings, preventing initial bioadhesion is a popular approach that generally involves the use of a hydrophilic polymeric coating. The concept is to present an interfacial steric barrier between the substrate and the environment in order to prevent conditioning layer dependent biofouling. Poly (ethylene glycol) (PEG) is widely used to functionalize surfaces in order to render them nonfouling. The osmotic and elastic properties of PEG along with its neutral charge, nontoxic nature make it an effective and safe choice to minimize fouling in a number of biologically relevant applications.[4] The ability for a given PEG functionalized surface to resist fouling is thought to be mainly dependent on the graft density and molecular weight (M_W) of PEG used, both of which are key properties that decide the conformation of PEG chains on surfaces.[5–7] For example. in the case of high or low graft density, PEG chains are arranged in either the "brush" or "mushroom" conformation, respectively.[8] A pancake conformation is observed for very low graft densities. Self-assembled monolayers (SAMs) of PEG chains are known to resist nonspecific adsorption best when present in the brush conformation.[7] Studies have shown that covalently immobilized PEG coatings provide superior antifouling properties, probably since they cannot easily be displaced by biomolecules or conditioning layer molecules.[9] PEG functionalization techniques can be broadly classified into "grafting to" and "grafting from" approaches. The grafting from technique generally gives higher graft density since the limiting factor is diffusion of monomer onto the reactive ends of growing chains, whereas in the case of the grafting to technique the limitation is diffusion of entire polymer chains to the reactive substrate.[10] Several strategies such as cloud point grafting,[11] grafting in homopolymer solutions,[12] grafting from polymeric melts,[13] and underbrush formation by backfilling with shorter molecules[14] have been used to increase the graft density for grafting to techniques. The backfilling approach, unlike the other three strategies that depend on minimization of excluded volume interactions, is a simple method wherein the interchain spaces present in layers of high M_W PEG chains are filled with shorter PEG chains that can diffuse to the surface. In a study of 5 kDa M_W PEG by Uchida and co-workers, it was shown that backfilling with shorter PEG (M_W 2 kDa) improved the ability of the surface to resist nonspecific protein adsorption.[14,15]

a)Authors to whom correspondence should be addressed; electronic addresses: ryo@phys.au.dk; pkingshott@swin.edu.au
b)Present address: Industrial Research Institute Swinburne (IRIS), Swinburne University of Technology, Burwood Road, Hawthorn 3122, Australia.

However, the mechanism of formation of mixed layers is not yet fully understood. The possibility of the formation of domains exists [Fig. 1(a)] where the mechanism of addition is similar to that of the replacement phenomena observed for short alkane thiol SAMs when they are exposed to longer alkane thiol molecules.[16] Here, replacement of short alkane thiol by longer alkane thiols begins at grain boundaries and is followed by gradual replacement of entire domains, resulting in phase separated arrangement.[16,17] The replacement of shorter alkane thiols with longer alkane thiols in SAMs is thermodynamically favored due to the higher number of intermolecular van der Waals interactions formed with longer alkane thiol molecule. Uchida and co-workers studied the backfilling of high M_W PEG layers with low M_W PEG and assumed that the addition of low M_W species results in formation of well-mixed, homogeneous mixed layers[14,15] The aspect of replacement and the extent of replacement are expected to be low since it is thermodynamically unfavorable for a longer PEG molecule to be replaced by a shorter PEG molecule. Examples of backfilling studies other than ethylene glycol related SAMs can be found in literature. For instance, Herne and Tarlov backfilled SAMs of thiolated deoxyribonucleic acid (DNA) strands using mercaptohexanol[18] and found that physically adsorbed DNA strands were replaced upon backfilling due to desorption caused by mercaptohexanol addition. Brunner *et al.* observed the formation of phase separated islands when SAM of poly(*p*-phenylene) was exposed to octadecane thiol.[19] Lee *et al.* conducted backfilling studies on monolayers of thiol functionalized single strand DNA on gold with 11-mercapto-1-udecanol (Ref. 20) and also using oligo (ethylene glycol) (OEG) terminated 11-mercapto-1-udecanol molecules.[21] In both backfilling studies they observed initial incorporation of alkane thiol or OEG thiol into vacant sites present in SAMs of thiolated DNA, however upon prolonged exposure the DNA molecules were desorbed from the SAM due to replacement by alkylthiol or OEG thiol molecules.

Here we have used OEG terminated alkane thiols to backfill PEG thiol SAMs on Au surfaces. The alkane thiol SAM formation is driven by intermolecular van der Waals interactions and is also kinetically more reactive than high M_W PEG thiols. Our aim is to thoroughly explore whether phase separated domains are formed [Fig. 1(a)] and also the extent of PEG desorption. The schematic presentation of thiolated PEG, OEG, and alkane molecules is presented in Fig. 1(c). Although SAMs of OEG have been shown to be very efficient in resisting protein adsorption[22] for short durations, it has been identified that applications involving immobilization of bioactive molecules such as enzymes would benefit from longer PEG chains due to higher mobility for biorecognition.[23] Thus we expect our combination of PEG-COOH$_{SAM}$ backfilled with OEG$_3$ will be an ideal support for immobilizing bioactive molecules.

We will use the following notations for SAM of PEG and for the backfilled surface:

(1) PEG-COOH$_{SAM}$, OEG$_{3-SAM}$, and R$_{SAM}$ correspond to SAMs formed with PEG-COOH, OEG$_3$, and R molecules.

(2) PEG-COOH$_{SAM}$ + OEG$_3$:PEG-COOH$_{SAM}$ backfilled with OEG$_3$.

(3) PEG-COOH$_{SAM}$ + R:PEG-COOH$_{SAM}$ backfilled with R.

II. MATERIALS AND METHODS

A. Chemicals

α-Carboxyl-ω-thiol poly(ethylene glycol) (PEG-COOH, M_W 2000 Da, 99% purity) was purchased from Laysan Bio Inc. (Arab, AL), and hydroxy-terminated tri (ethylene glycol) undecane thiol (OEG$_3$, 99% purity) was purchased from Asemblon (Redmond, WA). Fetal bovine serum (FBS), octane thiol (R) (99% purity), SYBR Green II, phosphate buffered saline (PBS) buffer tablets, 25% ammonium hydroxide (NH$_4$OH), 30% hydrogen peroxide (H$_2$O$_2$), and absolute ethanol were purchased from Sigma Aldrich (Aarhus, Denmark). Ultrapure MilliQ (MQ) water with resistivity of 18.2 MΩ was used for making buffers and aqueous ethanolic solutions.

B. Substrate preparation and functionalization

Gold substrates were prepared by sputtering 50 nm gold layer onto a 3 nm titanium adhesion layer on silicon wafers. Sputtering was done using an rf sputtering system with Ti and Au targets of 10 cm diameter (2.54 W cm^{-2}) inside a standard chamber maintained at an Ar pressure of 2×10^{-3} mbar. The substrate–target separation distance was 7 cm, while the deposition rates for Ti and Au were 0.4 and 1 nm s^{-1}, respectively. The gold surfaces were cleaned by UV/ozone treatment for 30 min, followed by treatment with basic piranha solution (H$_2$O: NH$_4$OH: H$_2$O$_2$ in ratio 4:1:1) at 70–80 °C for 5 min and then rinsed with MQ water. (CAUTION: Piranha solution reacts violently upon contact with organic solutions.) Cleaned gold slides were immersed for 3
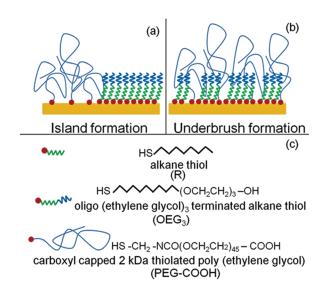

FIG. 1. (Color online) Schematic diagrams of backfilled PEG SAM in island type (a) and underbrush type arrangements (b). (c) The chemical formula and assigned abbreviations for various molecules used in self-assembly and backfilling experiments.

h at room temperature in 0.2 mM PEG-COOH solution (75% ethanol), followed by rinsing with MQ water to remove any physically adsorbed molecules. Backfilling involved immersion of PEG-COOH$_{SAM}$ for 3 h at room temperature in 1 mM absolute ethanolic solution of OEG$_3$ or R, followed by rinsing with ethanol and drying with a jet of nitrogen. The SAMs of OEG$_3$ and R for control experiments were made by immersing cleaned gold slides in 1 mM ethanolic solution of OEG$_3$ or R for a period of 3 h followed by rinse with ethanol and drying with nitrogen gas.

C. X-ray photoelectron spectroscopy

All spectra were recorded using a Kratos Axis Ultra^{DLD} instrument (Kratos Ltd, Telford, UK) equipped with a monochromated aluminum anode (Al $K\alpha$ 1486 eV) operating at 150 W power (15 kV and 10 mA) with pass energies of 80 and 160 eV for high resolution and survey spectra, respectively. A hybrid lens mode was employed during analysis (electrostatic and magnetic). The spectra were measured at three areas on each sample and the photoelectron take-off angle with respect to the normal to the surface in all measurements was 0°.The measured binding energy positions were charge corrected with reference to 285.0 eV, corresponding to the C–C/C–H species. Quantification and curve fitting was conducted using CASAXPS software. A linear background with a Gaussian to Lorentzian ratio of 30 was used to fit all spectra. The S $2p$ high resolution spectra were peak fitted into two doublets corresponding to bound and unbound thiol each with full width half maximum of 1.2 eV. The lower binding energy doublet with its $2p_{3/2}$ at 161.9 eV was assigned to bound thiol, while the higher binding energy doublet with its $2p_{3/2}$ at 163.5 eV corresponded to unbound thiol as described by Castner *et al.*[24] The representative high resolution spectra are included in Ref. 25 (Fig. S1b). Overlayer thickness and graft density were calculated using Eqs.(1)–(3).[5,6,26] Additional information on the calculation of inelastic mean free path of Au $4f$ photoelectron is included in Ref. 25,

$$\frac{I}{I_0} = \exp\left(\frac{-d}{\lambda\,\sin\,\theta}\right), \tag{1}$$

$$\lambda = \lambda_i(E_{KeV})^{0.79}, \tag{2}$$

$$L = \left(\frac{M}{\rho N_A d}\right)^{1/2}, \tag{3a}$$

$$S = \frac{1}{L^2}, \tag{3b}$$

where I_0 is the signal intensity from bare infinitely thick substrate (assumed to be 100%), I is the substrate signal after functionalization, d is the overlayer thickness, λ is the inelastic mean free path (IMFP) of Au $4f$ photoelectron in PEG polymer, θ is the photoelectron take-off angle with respect to normal to the surface, λ_i is the IMFP of 1 keV electron

through PEG (Cumpson[26]), E_{KeV} is the kinetic energy of photoelectron in keV, L is the interchain distance, M is the molecular weight of PEG chain, ρ is the density assumed to be 1 g/cm^3, N_A is the Avogadro number, and S is the graft density defined as number of chains per unit area.

D. Contact angle measurements

Static contact angles were measured on all surfaces using water, formamide, and α-bromonapthalene. All images of liquid drops on surfaces were recorded using a KRUSS DSA100 (KRUSS GmbH, Hamburg, Germany), followed by drop shape analysis using IMAGEJ software. Reported contact angles are the average of at least six measurements at different surface positions (data are included in Ref. 25, Table SIa). The values of γ_L^d, γ_L^+, γ_L^- for the three liquids used are given in Ref. 25 (Table SIb). The interfacial Lifshitz–van der Waals (γ^d) and polar components (γ^+, γ^-) of surface tension of a surface can be determined by measuring contact angles with three different liquids followed by solving the corresponding equations whose general form is given by[27]

$$(1 + \cos\,\theta)\gamma_L = \frac{1}{2}\left[\left(\gamma_S^d\gamma_L^d\right) + \left(\gamma_S^+\gamma_L^-\right) + \left(\gamma_S^-\gamma_L^+\right)\right] \tag{4}$$

θ is the measured contact angle. γ_L, γ_L^d, γ_L^+, and γ_L^- represent total surface tension, Lifshitz–van der Waals component, electron acceptor component, and electron donor component of liquid, respectively. γ_S, γ_S^d, γ_S^+, and γ_S^- represent total surface tension, Lifshitz–van der Waals component, electron acceptor component, and electron donor component of sample surface, respectively.

E. Atomic force microscopy

All images were recorded using a commercial Nanoscope VIII MultiMode SPM system (Bruker AXS, Santa Barbara, CA) in MQ water. Topography images were recorded using Quantitative Nano-Mechanical Mapping (QNM) under Peak-force Tapping mode.[28] Ultrasharp silicon nitride cantilevers (triangular, Mpp-12120-10, Bruker AXS) were used with a typical resonance frequency of 150 kHz in air, a spring constant of 5 N/m, and a normal tip radius of 8 nm. All atomic force microscopy (AFM) images were recorded with 512×512 pixels resolution per image, and they were flattened and analyzed with SCANNING PROBE IMAGE PROCESSOR software (SPIP^{TM}, Image Metrology ApS, version 5.1.3, Lyngby, Denmark).

F. Quartz crystal microbalance with dissipation

Quartz crystal microbalance studies were performed using a Q-Sense E4 system (Gothenburg, Sweden). The PEG-COOH functionalization followed by backfilling with OEG$_3$ or R was performed on QSX 301 crystals (Q-Sense) coated with 100 nm gold, which had approximate resonance frequency of 5 MHz. Serum adsorption experiments were performed in triplicate. Functionalized gold coated crystal surfaces were equilibrated at 37 °C in PBS (100 mM *p*H 7.4)

prior to exposure to serum solution. All serum adsorptions studies were carried out using 10% FBS at 37 °C. Once a stable baseline was attained, the surfaces were exposed to 750 μl of protein solution delivered at a flow rate of 100 μl/min followed by rinse with PBS buffer. The shift in resonance frequency corresponding to the seventh overtone was used to monitor the adsorption. After measurement, QCM crystals exposed to serum were rinsed with MQ water to remove any salts before drying under a jet of nitrogen for XPS analysis.

G. Bacterial adhesion assay

A *Staphylococcus aureus* (ATCC 12598) starter culture was inoculated from agar plates and grown in 3 ml of 1% tryptic soy broth (TSB) medium in 50 ml conical bottom tube by incubating overnight in a shaker at 37 °C. An inoculum prepared by adding 1 ml of starter culture to 100 ml 1% TSB medium was incubated in a shaker at 37 °C until cultures were in the late-exponential growth phase [optical density at 600 nm (OD600) (OD600 = 1.0)]. Cells were then harvested by centrifugation (5 min at 3000g), washed twice, and resuspended in PBS (pH 7.4) and diluted to obtain an OD_{600} of 0.5. Surfaces were incubated with the bacterial suspensions in 24 well plates for 5 h at 37 °C and gently washed three times with sterile PBS to remove nonadherent cells. The adherent cells on the surfaces were stained with ~10 μl 20x SYBR Green II RNA stain (2 μl ml^{-1} of 10.000x SYBR Green II stock), covered with glass cover slips and sealed with nail polish to avoid evaporation. Slides were stored in the dark at 4 °C until analyzed. Adherent cells were counted by fluorescence microscopy using a Zeiss Axiovert 200M epifluorescence microscope (Carl Zeiss GmbH, Jena, Germany) equipped with Zeiss filter set 10 and 63x oil immersion objective. Cells were counted in 109 μm^2 grids on triplicates of sample on a total of 15 random positions on each surface type.

III. RESULTS AND DISCUSSION

A. Extent of addition and coverage in backfilled monolayer

XPS was used to monitor the chemical changes occurring on Au substrates functionalized with PEG-COOH upon exposure to OEG$_3$ or R molecules. The respective relative elemental and chemical species calculated from survey and high resolution XPS scans are summarized in Table I. The substrate photoelectrons are attenuated by the overlayer and hence the substrate signal has an inverse relationship with overlayer coverage as shown in Eq.(1). The Au 4f signal was used to obtain quantitative data on the addition of molecules to the PEG-COOH$_{SAM}$. The Au 4f signal of PEG-COOH$_{SAM}$ + OEG$_3$ is 3.6% lower than that of PEG-COOH$_{SAM}$, indicating that OEG$_3$ molecules have added to the PEG-COOH$_{SAM}$. From the chemical structure of OEG$_3$ and R molecules it can be observed that they have lower O/C and higher aliphatic peak (285.0 eV)/ether peak (286.7 eV) ratios when compared to PEG-COOH and hence any addition during backfilling results in a corresponding change in the detected O/C and aliphatic peak/ether peak ratios. The aliphatic peak/ether peak ratio was calculated from the peak areas of components corresponding to binding energies 285.0 eV (aliphatic) and 286.7 eV (ether) obtained from high resolution C 1s spectra shown Figure S1a of Ref. 25. Addition of OEG$_3$ is further supported by a decrease in O/C ratio from 0.49 to 0.42 and increase in aliphatic peak/ether peak ratio from 0.1 to 0.3 as shown in Table I. The PEG-COOH$_{SAM}$ + R system exhibits a decrease in O/C ratio from 0.49 to 0.40 and increase in aliphatic peak/ether peak ratio from 0.1 to 0.4 similar to PEG-COOH$_{SAM}$ + OEG$_3$, except for the Au signal which increased by 2.6%. The increase in substrate signal indicates a decrease in overlayer thickness that could be caused by desorption of some PEG-COOH molecules during backfilling by R molecules.

Based on O/C ratios obtained from XPS of PEG-COOH$_{SAM}$, OEG$_{3-SAM}$, and R$_{SAM}$, a change in O/C ratio as a function of relative coverage of PEG-COOH and OEG$_3$ or R was plotted assuming a linear relationship (Fig. 2). By correlating the experimentally obtained values of O/C ratios for PEG-COOH$_{SAM}$ + OEG$_3$ and PEG-COOH$_{SAM}$ + R, we estimate the coverage of OEG$_3$ or R on the backfilled PEG-COOH$_{SAM}$ surface to be 29% and 18%, respectively. It must be noted that this estimation assumes that the intermolecular spaces in PEG-COOH$_{SAM}$ are contamination free, which in real laboratory conditions is not the case and thus we overestimate the number of added molecules. Here, however, we mainly focus on the relative differences rather than the absolute values. Despite the greater number of OEG$_3$ molecules being added

TABLE I. Summary of XPS results.

Sample	PEG-COOH$_{SAM}$	OEG$_{3-SAM}$	R$_{SAM}$	PEG-COOH$_{SAM}$ + R	PEG-COOH$_{SAM}$ + OEG$_3$
Au %[a]	38.95 ± 0.38	32.56 ± 0.35	55.3 ± 2.4	41.56 ± 0.45	36.23 ± 0.50
O/C[b]	0.49 ± 0.03	0.25 ± 0.01	0.0 ± 0.0	0.40 ± 0.01	0.42 ± 0.01
Aliphatic/ether[c]	0.13 ± 0.01	0.84 ± 0.02	21.19 ± 0.08	0.37 ± 0.01	0.30 ± 0.00
S %[d]	2.10 ± 0.20	1.53 ± 0.15	3.23 ± 0.41	2.06 ± 0.20	1.90 ± 0.60
% bound S[e]	78.26 ± 0.69	80.70 ± 1.03	88.14 ± 1.02	81.76 ± 0.95	79.86 ± 0.65

[a]Relative atomic percentage of Au.
[b]Ratio of relative atomic percentage oxygen and carbon.
[c]Aliphatic/ether—ratio of aliphatic (285.0 eV) and ether (286.7 eV) components in the C 1s high resolution spectra.
[d]Relative atomic percentage of S.
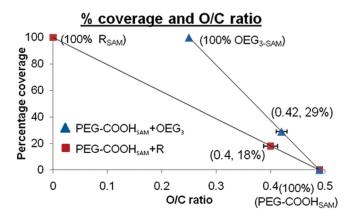[e]Percentage of bound sulfur from components in S 2p high resolution spectra.

FIG. 2. (Color online) Relative coverage of PEG-COOH and R or OEG$_3$ on backfilled surfaces as determined by correlating their XPS O/C ratios (on X axis) to a plot obtained by extrapolating values of O/C ratio for 0% and 100% relative coverage (on Y axis) assuming a linear relationship. The data points triangle and square shown in the plot represent the experimentally obtained O/C ratios for PEG-COOH$_{SAM}$ + OEG$_3$ and PEG-COOH$_{SAM}$ + R, respectively.

TABLE II. Surface tension components: the Lifshitz–van der Waals component (γ_S^d), electron acceptor component (γ_S^+), and electron donor component (γ_S^-) determined from the surfaces of OEG$_{3\text{-SAM}}$, R$_{SAM}$, PEG-COOH$_{SAM}$, PEG-COOH$_{SAM}$ + R, and PEG-COOH$_{SAM}$ + OEG$_3$.

Sample	γ_S^d (mJ/m^2)	γ_S^+ (mJ/m^2)	γ_S^- (mJ/m^2)
OEG$_{3\text{-SAM}}$	43.45 ± 0.06	0.85 ± 0.05	45.66 ± 1.49
R$_{SAM}$	30.67 ± 1.27	0.01 ± 0.01	0.69 ± 0.26
PEG-COOH$_{SAM}$	44.24 ± 0.04	0.92 ± 0.05	43.97 ± 1.56
PEG-COOH$_{SAM}$ + R	44.05 ± 0.08	0.96 ± 0.03	36.58 ± 0.80
PEG-COOH$_{SAM}$ + OEG$_3$	44.07 ± 0.1	0.90 ± 0.05	42.90 ± 1.59

to the PEG-COOH$_{SAM}$, the decrease in carboxyl peak area (Table I) in C $1s$ spectra of PEG-COOH$_{SAM}$ + OEG$_3$ and PEG-COOH$_{SAM}$ + R are comparable. This suggests that desorption of PEG-COOH is lower when OEG$_3$ is added in comparison to when R is added. The amount of S in PEG-COOH$_{SAM}$ was 2.1%, which is higher than the corresponding stoichiometric ratio of < 1%, very similar to what was reported by Unsworth *et al.*[8] with hydroxyl terminated 2 kDa PEG thiol molecules under cloud point conditions. It was suggested by Unsworth *et al.*[8] that relative atomic percentage of S from SAMs of PEG thiol depends not only on the stoichiometric ratio but also on the extent of dehydration and collapse of brushes during grafting of chains as described by Unsworth *et al.*[8] An alternate explanation for the high S% could be due to the presence of short thiolated impurities with higher S/C ratio when compared to that of PEG-COOH molecule. Though R and OEG$_3$ molecules have S/C ratios of 0.11 and 0.045, respectively, which is higher than the ratio for PEG-COOH$_{SAM}$ (0.008), the backfilling of PEG-COOH$_{SAM}$ with either R or OEG$_3$ did not significantly change the relative atomic percentage of S (Table I). Hence, the S content was not helpful in providing additional information about the backfilling process. The percentages of bound thiol on functionalized surfaces were determined as described earlier in the methods Sec. II C. The amount of bound sulfur was found to increase by a small extent (increase of 3.5%) upon backfilling PEG-COOH$_{SAM}$ with R, and for OEG$_3$ it increased by 1.6%. This small increase in bound sulfur could be due to Au–thiol bond formation of backfilled molecules, also indicating that a significant proportion of added molecules have chemisorbed to the gold surface and not physically adsorbed. The peak fitted high resolution S $2p$ spectra of various samples are included in Ref. 25 (Figure S1b).

B. Arrangement of backfilled molecules

As discussed earlier, backfilling process could result in mixed monolayer with two possible arrangements, namely

underbrush and island. We used contact angle based surface energy measurements to find out the arrangement of backfilled molecules. Contact angle measurements have very high surface sensitivity (< 1 nm)[29] and allow the determination of the surface energy of materials.[27] The components of surface tension can be calculated by measurement of contact angles of three different liquids using Eq. (4).[27] The contact angles measured for various surfaces using three liquids are given in Ref. 25 (Table SIb). The surface tension components; Lifshitz–van der Waals component (γ_S^d), electron acceptor component (γ_S^+), andelectron donor component (γ_S^-) for various surfaces are shown in Table II. The hydrophobicity of a surface is determined by its γ_S^d value, and the lower the value, the more hydrophobic a surface is. Since alkane thiol molecules are hydrophobic an SAM of alkane thiol would have lower γ_S^d value than PEG or OEG based SAMs and this is apparent for the values determined for R$_{SAM}$ and OEG$_{3\text{-SAM}}$ (Table II). If alkane thiol molecules form islands instead of being homogeneously mixed during the backfilling of the PEG-COOH, then the γ_S^d value of PEG-COOH$_{SAM}$ + R would significantly decrease. The γ_S^d value 44.0 mJ/m^2 for PEG-COOH$_{SAM}$ + R is virtually the same as that of PEG-COOH$_{SAM}$ that has a γ_S^d value 44.0 mJ/m^2, indicating that hydrophobic islands are not present. The γ_S^- value of a surface gives a quantitative idea about the presence of electron donor groups, with the greater the value of γ_S^- the higher the number of surface electron donor groups. PEG and OEG have oxygen atoms and thus have higher γ_S^- values when compared to the alkane thiol (Table II). Backfilling PEG-COOH$_{SAM}$ with R results in a 7 mJ/m^2 decrease in γ_S^-, indicating that a significant number of PEG-COOH molecules have desorbed from the surface. The values for γ_S^d and γ_S^- for PEG-COOH$_{SAM}$ after addition of OEG$_3$ do not change significantly since both molecules have very similar values and could not easily be followed by contact angle measurements.

C. AFM results

QNM-AFM has a very high lateral resolution and has been used to characterize the surface morphology of the different SAM layers with the aim to check the presence of phase separated domains. With the use of the peak forces less than 1 nN, QNM-AFM is able to map mechanical properties of surfaces quantitatively while simultaneously
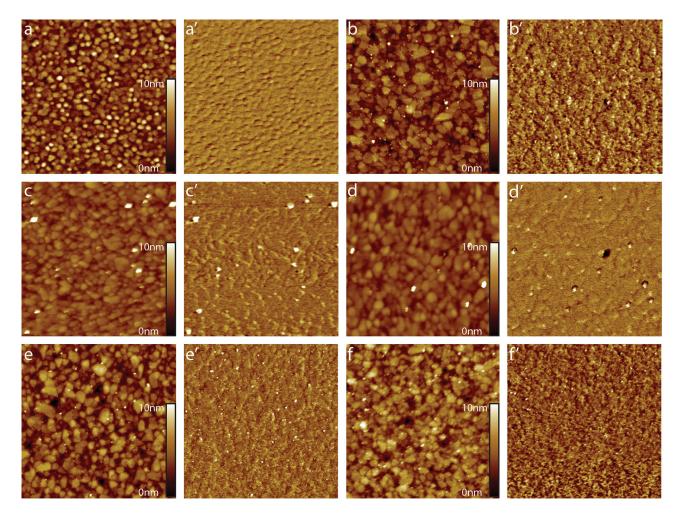
FIG. 3. (Color) Topography and Young's modulus images recorded by QNM-AFM measurements in MQ water. (a), (a′) Au substrate. (b), (b′) PEG-COOH$_{SAM}$. (c), (c′) OEG$_{3\text{-}SAM}$. (d), (d′) R$_{SAM}$. (e), (e′) PEG-COOH$_{SAM}$ + OEG$_3$. (f), (f′) PEG-COOH$_{SAM}$ + R. The scan area of each image is $1 \mu m \times 1 \mu m$.

capturing topographic images with the same resolutions as traditional tapping mode AFM (Refs. 28 and 30). All QNM-AFM measurements were done in liquid (MQ). The topography and modulus images of Au surface and various SAMs are shown in Fig. 3, and the corresponding surface roughness is summarized in Table III. The topography of the bare Au surface [Fig. 3(a)] shows Au grains without any additional features on top of grains. The recorded nanomechanical map of Au surface [Fig. 3(a′)] demonstrates the homogeneous Young's modulus distribution throughout the scanned area

TABLE III. Normalized surface roughness (to Au) values for OEG$_{3\text{-}SAM}$, R$_{SAM}$, PEG-COOH$_{SAM}$, PEG-COOH$_{SAM}$ + R, and PEG-COOH$_{SAM}$ + OEG$_3$.

Sample	Roughness (Sq) (nm)	Sq$_{SAM}$/Sq$_{Au}$[a]
PEG-COOH$_{SAM}$	0.69 ± 0.04	1.44
OEG$_{3\text{-}SAM}$	0.63 ± 0.04	1.31
R$_{SAM}$	0.21 ± 0.02	0.44
PEG-COOH$_{SAM}$ + OEG$_3$	0.81 ± 0.05	1.69
PEG-COOH$_{SAM}$ + R	0.66 ± 0.06	1.38

[a]Sq$_{SAM}$/Sq$_{Au}$ is the ratio of the means of the two surface roughness; Sq$_{Au}$ = 0.48 ± 0.02 nm.

has nearly the same range of stiffness showing the same color contrast. Comparing the topography images of modified surfaces with bare Au, one can clearly see the additional particlelike features on all modified surfaces [igs. 3(b)–3(f)]. In addition, the modulus images of the modified surfaces show that the grain boundaries are less visible due to the SAMs. Interestingly, the modulus of the modified surfaces also represents the surface modulus variations, because of the slightly different color contrast [Figs. 3(b′)—3(f′)]. The small variations in material properties observed in elastic modulus measurements are particularly useful in the analysis of heterogeneous surface. However, most important, phase separations were not observed in any AFM image of back-filled PEG-COOH$_{SAM}$. This indicates that the backfilled surfaces are homogeneous. Hence we conclude that both OEG$_3$ and R molecules form homogeneous mixed layer upon addition to PEG-COOH$_{SAM}$. Furthermore, the surface roughness changed dramatically after modification. The surface roughness of PEG-COOH$_{SAM}$ increases by 0.12 nm upon exposure to OEG$_3$ molecules. Lee *et al.*[21] showed that the proportion of DNA molecules in upright orientation in an SAM of thiolated single strand DNA on gold increased upon exposure to OEG terminated alkane thiol molecules. An

increase in proportion of PEG molecules in upright orientation could explain the increase in surface roughness of PEG-COOH$_{SAM}$ upon exposure to OEG$_3$. Lee *et al.*[20] showed that addition of alkylthiol molecules onto SAM of thiolated single strand DNA on gold increased the fraction of DNA molecules in upright orientation. There was no increase in roughness value during the addition of R onto PEG-COOH$_{SAM}$, in fact the surface roughness of PEG-COOH$_{SAM}$ + R decreases by 0.03 nm (decrease within the error; hence not significant). It must be noted that the addition of R caused more desorption of PEG-COOH molecules when compared to that observed during the addition of OEG$_3$. Thus desorption of PEG-COOH molecules during the addition of R could be the reason behind the surface roughness of PEG-COOH$_{SAM}$ + R not being higher than PEG-COOH$_{SAM}$.

D. Fouling resistant properties of PEG-COOH surfaces with and without underbrush

Resistance towards nonspecific adsorption can be tested using simple model systems such as single protein solutions. Examples have included collagen (Ref. 31) and bovine serum albumin.[32] More rigorous tests are conducted with serum[32] or microbial cell suspensions.[33] The protein adsorption resistant properties of the PEG-COOH$_{SAM}$ and mixed surfaces were evaluated by serum adsorption and bacterial adhesion studies. The addition of smaller OEG chains in theory increases the
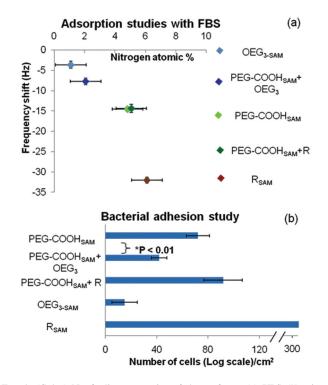

graft density of protein resistant molecules within the layer of diffuse PEG-COOH$_{SAM}$ and hence is expected to improve its resistance towards nonspecific adsorption.

QCM and XPS have been employed to quantitatively compare the serum adsorption resistant properties of the SAMs. The frequency shift after serum exposure in QCM is directly proportional to the amount of protein adsorbed,[32] and the relative atomic percentage of nitrogen from XPS also enables a quantitative estimation of the amount of adsorbed protein.[31] In Fig. 4(a) we show the data points corresponding to various samples studied, where the X axis shows the % N obtained from XPS and the Y axis shows the frequency shift from the QCM data. Upon serum exposure the QCM frequency decreases by 7 Hz for the PEG-COOH$_{SAM}$ + OEG$_3$ surface, compared to the PEG-COOH$_{SAM}$ and PEG-COOH$_{SAM}$ + R surfaces, which both exhibit a frequency shift of about 15 Hz. The lower frequency shift for PEG-COOH$_{SAM}$ + OEG$_3$ proves that OEG$_3$ addition improves the protein adsorption resisting ability of PEG-COOH$_{SAM}$. We also speculate that protein adsorption would be lower if the PEG thiol molecules used did not have a carboxyl end-group, increasing electrostatic interactions with oppositely charged serum proteins and facilitating higher adsorption. Representative QCM kinetic plots are included in Ref. 25 (Fig. S2). Figure 4(a) also shows the nitrogen content on the X axis, where the PEG-COOH$_{SAM}$ + OEG$_3$ surface has 2% N compared to PEG-COOH$_{SAM}$ and PEG-COOH$_{SAM}$ + R surfaces both showing approximately 5% N, which follows the same trend as seen with QCM. The OEG$_{3-SAM}$ had the highest ability to resist serum adsorption, which agrees with previous studies with OEG based SAMs.[22] The serum adsorption on R$_{SAM}$ is the highest (33 Hz shift) among all the surfaces tested in this study, this could most likely be attributed to the significantly higher hydrophobicity of SAM of alkane thiol.

The surfaces were tested for bacterial adhesion using a *Staphylococcus aureus* strain and the results are shown in Fig. 4(b). Clearly, the PEG-COOH$_{SAM}$ + OEG$_3$ (4.2×10^7 cells/cm^2) surface is better at resisting bacterial adhesion when compared to PEG-COOH$_{SAM}$ (7.2×10^7 cells/cm^2) and PEG-COOH$_{SAM}$ + R (9.2×10^7 cells/cm^2). Hence it can be concluded that adding OEG$_3$ molecules improves the ability of PEG-COOH$_{SAM}$ to resist fouling. R$_{SAM}$, being highly hydrophobic, had the highest bacterial attachment count when compared to all other surfaces tested for bacterial adhesion in this study. Though the OEG$_{3-SAM}$ has the least bacterial adhesion and serum adsorption, we propose that PEG-COOH$_{SAM}$ + OEG$_3$ system would be a better surface for applications involving immobilization of bioactive molecules such as enzymes and further advantages of PEG-COOH$_{SAM}$ + OEG$_3$ are discussed in the following.

E. Discussion

We have studied a mixed monolayer of OEG$_3$ on PEG-COOH$_{SAM}$ using XPS, contact angle, and AFM. The contact angle results support the notion that phase separated surface

F$_{IG}$. 4. (Color) Nonfouling properties of the surfaces. (a) XPS (X axis—N%) and QCM (Y axis—frequency shift) based quantification after exposure to 10% FBS adsorption, to PEG-COOH$_{SAM}$, PEG-COOH$_{SAM}$ + R, and PEG-COOH$_{SAM}$ + OEG$_3$, OEG$_{3-SAM}$, and R$_{SAM}$ surfaces. (b) Results of bacterial adhesion studies using *Staphylococcus aureus* performed on PEG-COOH$_{SAM}$, PEG-COOH$_{SAM}$ + R, and PEG-COOH$_{SAM}$ + OEG$_3$, OEG$_{3-SAM}$, R$_{SAM}$. The X axis shows the number of adherent cells on the log scale.

arrangement of the two molecules does not occur, proving that homogeneous mixed layers are formed. There have been some reports on grafting 2 kDa PEG thiol chains. For example Unsworth *et al.*[8] reported a maximum graft density of 0.58 chains/nm^2 using methoxy capped 2 kDa PEG thiol chains under cloud point conditions, and Tokumitsu *et al.*[34] reported a maximum graft density of 3.6 chains/nm^2 using 2 kDa PEG conjugated to undecane thiols. Theoretical maximum graft density that can be obtained using PEG SAM is 4.8 chains/nm^2, assuming the molecular cross-sectional area for PEG brush in helical conformation to be 22 Å^2 as reported by Harder *et al.*[22] From XPS data we have calculated a graft density of PEG-COOH$_{SAM}$ to be 1.0 chain/nm^2 using Eqs. (1)–(3). Thus, the PEG-COOH chains in PEG-COOH$_{SAM}$ have a density that is not close-packed and there exists sufficient space for the smaller OEG molecules to fill the gaps, although in a good solvent the PEG is likely to extend and form highly mobile brushes.[8]

We used carboxyl capped PEG molecules since we intend to use them for immobilization of antibacterial enzymes in future studies. The carboxylic groups are expected to contribute to the surface negative charge. We suspect that the nonfouling properties would be better with hydroxyl or methoxy capped PEG molecules, which are neutrally charged and thus minimize electrostatic interactions. Our mixed PEG-COOH$_{SAM}$ + OEG$_3$ system is anticipated to be an ideal platform for immobilization of bioactive molecules, since the OEG maximizes nonfouling potential while the longer PEG chains would confer higher mobility and thus improved bioactivity capabilities to the immobilized molecule.[23] There have been reports on bacterial adhesion studies on OEG (Ref. 35) and PEG (Ref. 33) surfaces. Our adhesion studies with *Staphylococcus aureus* involved different incubation time compared to that used by Nejadnik *et al.*,[33] also Ostuni *et al.*[35] used a counting technique involving removal of attached cells by sonication followed by counting the colony forming units on culture plates that introduce the possibility of tenfold error in estimation as mentioned by authors. Hence, the absolute values of our bacterial adhesion studies could not be compared with these earlier reported studies. We plan to immobilize enzymes on backfilled PEG-COOH$_{SAM}$ + OEG$_3$ surfaces and further understand the role of backfilled OEG molecules.

IV. SUMMARY AND CONCLUSIONS

We have investigated backfilling of a PEG-COOH$_{SAM}$ with alkane and oligo ethylene glycol terminated thiol molecules. From XPS and contact angle results we have shown that R molecules form mixed layers and the addition process is accompanied by desorption of PEG-COOH molecules. OEG$_3$ molecules, upon addition, also formed mixed layers but less desorption of the PEG occurs, when compared to addition of R molecules. The nonfouling properties of various surfaces were compared, and it was shown that the PEG-COOH$_{SAM}$ + OEG$_3$ surface was found to be better than the PEG-COOH$_{SAM}$ surface with

respect to resisting serum adsorption and bacterial adhesion. Thus, the strategy involving backfilling using OEG terminating alkane thiols is indeed capable of improving the nonfouling properties of monolayers of PEG chains of significant graft densities.

[1]D. G. Castner and B. D. Ratner, Surf. Sci. **500**, 28 (2002).
[2]I. Banerjee, R. C. Pangule, and R. S. Kane, Adv. Mater. **23**, 690 (2010).
[3]K. Sauer, A. K. Camper, G. D. Ehrlich, J. W. Costerton, and D. G. Davies, J. Bacteriology **184**, 1140 (2002).
[4]S. I. Jeon, J. H. Lee, J. D. Andrade, and P. G. De Gennes, J. Colloid Interface Sci. **142**, 149 (1991).
[5]S. J. Sofia, V. Premnath, and E. W. Merrill, Macromolecules **31**, 5059 (1998).
[6]L. D. Unsworth, H. Sheardown, and J. L. Brash, Biomaterials **26**, 5927 (2005).
[7]L. D. Unsworth, H. Sheardown, and J. L. Brash, Langmuir **24**, 1924 (2008).
[8]L. D. Unsworth, Z. Tun, H. Sheardown, and J. L. Brash, J. Colloid Interface Sci. **281**, 112 (2005).
[9]P. Kingshott, J. Wei, D. Bagge-Ravn, N. Gadegaard, and L. Gram, Langmuir **19**, 6912(2003).
[10]N. Luo, J. B. Hutchison, K. S. Anseth, and C. N. Bowman, Macromolecules **35**, 2487 (2002).
[11]P. Kingshott, H. Thissen, and H. J. Griesser, Biomaterials **23**, 2043 (2002).
[12]W. Taylor and R. A. L. Jones, Langmuir **26**, 13954 (2010).
[13]S. Minko, S. Patil, V. Datsyuk, F. Simon, K.-J. Eichhorn, M. Motornov, D. Usov, I. Tokarev, and M. Stamm, Langmuir **18**, 289 (2002).
[14]K. Uchida *et al.*, Biointerphases **2**, 126 (2007).
[15]K. Uchida, H. Otsuka, M. Kaneko, K. Kataoka, and Y. Nagasaki, Anal. Chem. **77**, 1075 (2005).
[16]T. Kakiuchi, K. Sato, M. Iida, D. Hobara, S.-I. Imabayashi, and K. Niki, Langmuir **16**, 7238 (2000).
[17]G. G. Baralia, A.-S. Duwez, B. Nysten, and A. M. Jonas, Langmuir **21**, 6825 (2005).
[18]T. M. Herne and M. J. Tarlov, J. Am. Chem. Soc. **119**, 8916 (1997).
[19]S. Brunner *et al.*, Langmuir **15**, 6333 (1999).
[20]C.-Y. Lee, P. Gong, G. M. Harbers, D. W. Grainger, D. G. Castner, and L. J. Gamble, Anal. Chem. **78**, 3316 (2006).
[21]L. J. G. Chi Ying Lee, David W. Grainger, and David G. Castner, Biointerphases **1**, 11 (2006).
[22]P. Harder, M. Grunze, R. Dahint, G. M. Whitesides, and P. E. Laibinis, J. Phys. Chem. B **102**, 426 (1998).
[23]H. Otsuka, Y. Nagasaki, and K. Kataoka, Langmuir **20**, 11285 (2004).
[24]D. G. Castner, K. Hinds, and D. W. Grainger, Langmuir **12**, 5083 (1996).
[25]See supplementary material at http://dx.doi.org/10.1116/1.3647506 for the basis for calculating the value of inelastic mean free path of Au 4f photoelectrons through poly (ethylene glycol) using equation S1 and S2 is described in page 2. High resolution C 1s and S 2p x-ray photoelectron spectra of various mixed monolayer and control surfaces are presented in Figure S1. The contact angles for water, formamide and α-bromonapthalene measured on various mixed monolayer surfaces are shown in Table Sla. The Lifshitz van der Waals component (γ_S^d), electron acceptor component (γ_S^+), electron donor component (γ_S^-) of water, formamide and α-Bromonapthalene, the solvents used to calculate surface energy components, are presented in Table Slb. Representative QCM plots showing the change in frequency upon exposure to 10 % FBS on various mixed monolayer and control surfaces are presented in Figure S2.

[26]P. J. Cumpson, Surf. Interface Anal. **31**, 23 (2001).

[27]C. J. Van Oss, M. K. Chaudhury, and R. J. Good, Chem. Rev. **88**, 927 (1988).

[28]K. Sweers, K. van der Werf, M. Bennink, and V. Subramaniam, Nanoscale Res. Lett. **6**, 270 (2011).

[29]E. B. Troughton, C. D. Bain, G. M. Whitesides, R. G. Nuzzo, D. L. Allara, and M. D. Porter, Langmuir **4**, 365 (1988).

[30]B. Pittenger, N. Erina, and C. Su, *Quantitative mechanical property mapping at the nanoscale with PeakForce QNM Application Note*, Veeco Instruments Inc, Plainview, NY.

[31]M. A. Cole, H. Thissen, D. Losic, and N. H. Voelcker, Surf. Sci. **601**, 1716 (2007).

[32]B. Menz, R. Knerr, A. Göpferich, and C. Steinem, Biomaterials **26**, 4237 (2005).

[33]M. R. Nejadnik, H. C. van der Mei, W. Norde, and H. J. Busscher, Biomaterials **29**, 4117 (2008).

[34]S. Tokumitsu, A. Liebich, S. Herrwerth, W. Eck, M. Himmelhaus, and M. Grunze, Langmuir **18**, 8862 (2002).

[35]E. Ostuni, R. G. Chapman, M. N. Liang, G. Meluleni, G. Pier, D. E. Ingber, and G. M. Whitesides, Langmuir **17**, 6336 (2001).